LA-UR-23-24637

Approved for public release; distribution is unlimited.

Title:	Investigating the Role of Defects in -Pu Phase Transitions using Density Functional Theory
Author(s):	Boden, Samuel Bishop
Intended for:	Submission for undergraduate CAPSTONE research project.
Issued:	2023-05-01

Investigating the Role of Defects in α-Pu Phase Transitions using Density Functional Theory

Samuel B Boden

LA-UR-23-xxxxx
25 April 2023

Abstract

Before reaching its relatively low melting point of 913 K, plutonium undergoes six solid state phases: simple monoclinic alpha, body-centered monoclinic beta, face-centered orthorhombic gamma, face-centered cubic delta, body-centered tetragonal delta-prime, and body-centered cubic epsilon phases. Due to their low symmetry, the monoclinic alpha and beta phases have not been studied extensively, however it has been previously hypothesized that the transition between alpha and beta is caused by defects in the lattices due to the incommensurate number of atoms. Additionally, the martensitic delta to alpha phase transformation in plutonium-gallium alloys induces an expanded alpha lattice known as alpha prime, most likely due to the insoluble gallium impurity atom. This work explores how defects such as plutonium interstitials and gallium interstitials and substitutionals may affect the alpha plutonium lattice, providing a better understanding of the mechanisms for the alpha-beta and martensitic phase transformations through density functional theory (DFT). Results indicate that plutonium interstitials within the alpha lattice induce beta features structurally and electronically, such as volume expansion and bonding changes, and gallium interstitials and substitutionals within the alpha lattice induce volume changes as observed experimentally in alpha prime.

1. Introduction

The element plutonium (Pu) exhibits many unusual properties that have been puzzling the materials science community for decades. Pu is known for its unstable nature and radioactive decay caused by self-irradiation [1]. Part of plutonium's unstable behavior comes from its 5f electrons. Pu metal undergoes six phase transitions before reaching its melting point of 913 K, as described in Figure 1. These solid-state phases exhibit different crystal structures, volume changes, and electronic structure properties. The ground state has a very low symmetry monoclinic structure with 16 atoms in its unit cell [2]. This phase is referred to as the alpha phase (α). In contrast, the high temperature delta (δ) phase has a high symmetry face-centered-cubic structure with 4 atoms in its unit cell. Gibbs free energy varies little between the solid Pu phases, where defects, impurities, and temperature will modify or eliminate intermediate phase transitions. This is due to the complex 5f electronic behavior, where Pu is located at the boundary of delocalized/localized electrons within the actinide series [1–2].

Extensive research has been performed regarding many of the transitions between these phases and the mechanisms responsible for the transitions [1–8]. However, there are certain solid Pu transitions that are currently not as well understood, such as the martensitic phase transformation from the δ phase to an expanded α phase, known as the alpha prime (α') phase. This transition occurs in metastable plutonium–gallium (Ga) alloys with Ga concentrations below 3 atomic percent (at. %), where the δ phase is stabilized to room temperature with Ga alloying, and upon cooling will transition to the α' phase by a ~20% volume change. The expansion into the α' phase has been hypothesized due to the insoluble Ga atom [3–6, 9–10].

Arguably the least understood transition in solid plutonium is the α → β transition (Figure 2). Plutonium's beta (β) phase is a body-centered monoclinic structure with 34 atoms in its unit cell, while the α phase is a simple monoclinic with 16 atoms in its unit cell. The asymmetry between these two monoclinic structures makes the mechanism responsible for the transition hard to determine. If the β unit cell contained 32 atoms, this transition would be easier to understand as the number of atoms would be commensurate between the two. Due to the unusual nature of this transition and the low symmetry of both structures, few studies have been performed regarding the mechanism behind it. A study performed by Mitchell et al. finds that the diffusion of interstitials is likely responsible for the transition between β and α, but notes that no additional research has been done to show this [7].

Per Mitchell et al. [7], the hypothesis of the role of defects could help in determining the mechanism of the α → β phase transition, and possibly the mechanism behind the expansion into the α' phase due to the Ga impurity. Pu interstitials within the α unit cell would produce grounds to transition to a 34-atom unit cell, as seen in the β phase. As for the expansion into the α' phase, substituting Ga atoms into the α unit cell or inserting them as interstitials into the cell could uncover more information about this expansion and the martensitic phase transformation from Ga-stabilized δ to α'.

These possibilities can all be explored systematically by employing density functional theory (DFT), a first-principles quantum mechanical theory in which calculations on many-body systems can be performed [11]. Properties of these systems are approximated by expressing the electronic Hamiltonian equation as a functional of the electron density [12]. Minimizing the functional approximates the ground-state energy of the system. As of now, the exact representation is not known for the exchange–correlation functional and is hence approximated by various functionals. Several of these functionals predict properties of the system very accurately. The first of these is known as a local density approximation (LDA) [13], which assumes a homogenous electron density for the system, and therefore requires the functional be evaluated at only one point [12–13]. LDA provides an accurate approximation

of ground-state energies at a low computational cost for lighter elements. However, due to its electronic nature and the severe deviation of its behavior from a homogenous electronic gas, Pu requires the use of a generalized gradient approximation (GGA) [14]. With this functional, the electron density is evaluated on a gradient, allowing for a more accurate approximation of the electron density for larger electronic systems such as elements of the actinide series.

This study explores the potential pathways of phase transitions between α-Pu and β-Pu, and how α expands into the α' lattice, by investigating the role of defects in α-Pu as the predicted means of the transition. Through the use of DFT, this work will identify how the α-Pu lattice responds to defects by introducing Pu atoms and Ga atoms into the α-Pu lattice at various interstitial and substitutional sites. This work concludes that defects in α-Pu influence significant structural and electronic changes reflecting trends seen in β-Pu and in the α' lattice, and therefore that defects in α-Pu serve as a viable explanation to the uncertainty behind the mechanisms of these transitions.

2. Computational Methodology

The Vienna Ab-initio Simulation Package (VASP) is a computational tool used to implement DFT-based calculations and was the tool of choice for this research due to its assumption of a pseudopotential for core electrons and planewaves for valence electrons. This makes for accurate calculations that run much faster than an all-electron code for instance [11, 15–18]. For this study, the Perdew-Burke-Ernzerhof (PBE) GGA functional was used throughout all calculations, due to its ubiquity in the field [17].

For a complete calculation, VASP requires four input files, named the INCAR, POTCAR, POSCAR, and KPOINTS. Each contains information specific to a certain aspect of a DFT calculation and as such VASP cannot be used without all four. The INCAR file describes the type of calculation performed and includes parameters such as specifying the functional, the energy and force convergence criteria, the type of relaxation performed, and multiple other attributes specific to DFT calculations. The POTCAR contains pseudopotential information for each atomic species used in the calculation, while the POSCAR defines atomic positions and lattice constants. The KPOINTS file describes how the Brillouin zone is to be sampled using the specified Bloch vectors, also known as a k-point mesh. For all simulations in this research, our theoretical α cell was sampled using an automatically generated 4 x 2 x 2 Monkhorst-Pack k-point mesh [3, 19]. The system was modeled as an antiferromagnetic (AFM) spin-polarized calculation with opposing magnetic moments and with zero total magnetic moment for the system. It has been shown that, for Pu, using a spin-polarized AFM arrangement compares more closely with experimental volume and energetics than non-spin-polarized (non-magnetic) calculations and spin-polarized (ferromagnetic) calculations without an AFM arrangement [20]. This will be furthered discussed below. Due to the extreme computational cost and no significant change in energetic trends, spin orbit coupling (SOC) was not implemented into these calculations [3].

Within the INCAR file are many flags detailing different aspects of how the calculation is to be performed, but the EDIFF, EDIFFG, and ENCUT flags are what define the convergence criteria for structural relaxations and energy minimization and are therefore important to discuss here. The EDIFF flag defines when the electronic minimization loop is to stop, meaning once the difference in total energy between two loop steps is less than the EDIFF value, electronic convergence has been reached. The EDIFFG flag specifies the force criterion for the ionic relaxation to stop, and these two parameters together dictate when the total calculation will converge. ENCUT defines the energy cutoff for the plane-wave-basis set. For this study, all calculations are considered converged with an

electronic convergence criterion of 10^{-6}eV, a force convergence criterion of 10^{-2} eV/Å, and a plane-wave cutoff of 550 eV.

Another important INCAR flag to discuss is the ISIF flag. This flag defines the method of structural relaxation. For this research, only ISIF = 2 and ISIF = 3 were used, where ISIF = 2 calls for a constrained structure relaxation — keeping the lattice volume constant but allowing the ionic positions to relax — and ISIF = 3 calls for a full cell relaxation, allowing not only the ionic positions to relax, but the cell volume and shape as well. ISIF = 2 and ISIF = 3 will be referred to as “dilute” relaxation and “full” relaxation, respectively.

Before any calculations involving defects in the α-Pu cell could be performed, a theoretical α-Pu structure needed to be defined at 0 K. This was done by first constructing a 1 x 2 x 1 α-Pu supercell to better reflect the lattice constants of the β unit cell, shown in Figure 3. As stated above, though Pu is non-magnetic experimentally [21], DFT predicts an antiferromagnetic ground state [22]. Due to this prediction and the low symmetry of the monoclinic structure, several AFM arrangements of the theoretical α supercell were tested (Figure 4) and relaxed using a full relaxation scheme to find the arrangement with the lowest total energy. Table 1 contains the results from these relaxations. It was found that arrangement #5 (AFM-5) exhibited the lowest total energy among all tested AFM arrangements, and therefore proceeded to serve as the theoretical α reference structure throughout the rest of this research. Our theoretical α cell yielded a volume of 572.71 $Å^3$, a contraction of 10.5% from the experimental 1 x 2 x 1 α supercell. This was the smallest volume change among all proposed AFM arrangements [1].

Having defined a theoretical reference structure for the α-Pu supercell, defect structures were then built from the reference structure. The first of these defects to be researched was Pu interstitials within the α-Pu matrix. As stated previously, two Pu interstitials in the α matrix would produce viable grounds to transition to a 34-atom β structure, and therefore each defect structure contained two Pu interstitials. Positioning of interstitials was determined by using the space group symmetry of the α structure and by using the β unit cell as a reference. In order to accommodate the Pu interstitial atom, the Pu–Pu bond distance was also taken into account, in which this distance had to be greater than 1.67 Å. Using these parameters, seven defected structures were defined (Figure 5). Each of the seven defected structures were then submitted to VASP for structural relaxation and energy minimization using the dilute relaxation scheme, indicating the energy required to accommodate the interstitial within the theoretical α-Pu lattice. Once converged, the relaxed structures were then submitted for full relaxation, indicating how the total volume and cell shape will change with the defects. When followed by a full relaxation, any internal pressure resulting from the introduction of the defects into the lattice will dissipate, bringing the internal pressure of the fully relaxed structure close to zero. The energy difference between the dilute relaxation and the full relaxation will provide an idea as to the amount of strain the defects are inducing on the α lattice. The formation energy for each interstitial (E_f) indicates the amount of energy in eV required for that defect to form on its own, and was determined using the following equation:

$$E_f = \frac{E_0 - \left(\frac{34}{32}\right) * E_{0t}}{2}$$

where E_0 is the total energy of the converged defect structure and E_{0t} is the total energy of the theoretical α supercell (AFM-5).

Simulated X-ray diffraction (XRD) patterns were plotted for each fully relaxed structure using the structure modeling software VESTA, before being transferred to OriginLab for further manipulation and

analysis [23–24]. The converged structures' XRD patterns were then compared to the XRD patterns for the experimental β structure and the theoretical α supercell to determine which interstitial defect structures had XRD peaks that more closely resembled β-phase XRD peaks, shown in Figure 10. Selected structures were then re-run in VASP as a single-point calculation (no convergence criteria) to produce partial density of states (PDOS) data for analysis of the electronic structure. For each structure, three atoms were compared using PDOS: the interstitial atom itself, the first nearest neighboring atom (1nn) to the interstitial, and that atom in the non-defected theoretical α structure. Figure 11 shows the PDOS for the 6d and 5f states of these atoms.

Using the same theoretical α supercell, Ga defects were introduced to explore the martensitic phase transformation to α'. The same suggested interstitial positions for Pu-defected structures were used to introduce Ga interstitials into the theoretical α supercell. Instead of introducing both interstitials at once, 14 defected structures were made using one Ga atom as an interstitial in each individual site of the 7 symmetric interstitial pairs (Figure 7). This yields a Ga concentration of 3.030 at. %. The α unit cell is arranged by an inverse symmetry operation resulting in 8 distinct atomic sites throughout the lattice. These 8 sites were used to substitute Ga atoms into the theoretical α supercell, creating 8 more defected structures with a Ga concentration of 3.125 at. % (Figure 6). Each of the 14 defected structures with Ga as interstitials and the 8 defected structures with Ga as substitutionals were then submitted for dilute relaxations following the same input methods as with the Pu interstitial structures. Once converged, the most energetically favorable defect structures (Table 5) were submitted for full relaxation. The fully relaxed structures had their XRD patterns analyzed and compared to the theoretical α cell as well as the experimental α' cell [1]. PDOS data was calculated using single-point calculations in VASP and again analyzed using OriginLab, where the Ga atom in each defected structure was compared to its 1nn Pu atom and that same Pu atom in the non-defected theoretical α cell, giving us insight into how the Ga atom affects the bonding of its neighboring Pu atoms. The XRD and PDOS results for fully relaxed Ga-defected structures can be seen in Figure 12 and Figure 13, respectively.

3. Results and Discussion

3.1. α-Pu Interstitials – Dilute Relaxations

3.1.1. Energetics.

The resulting formation energies for each defected structure in the dilute relaxations are shown in Table 2, with defect structure Pu-6 being the most energetically favorable at 2.586 eV per interstitial (eV/int). Structure Pu-3 was the least energetically favorable at 4.582 eV/int. Table 2 also shows each formation energy relative to Pu-6 (dE_f). From this we can see that the dilute formation energies have a range of 1.996 eV/int. The defected structures with lower formation energies are more likely to appear in experiment, making Pu-6 the most likely defected structure to emerge and Pu-3 the least. This sets up a potential pathway for diffusion from α to β, which will be discussed in section 3.2.4.

3.1.2. Structural Analysis.

All relaxed defect structures were analyzed and compared to the β unit cell in Figure 8, where similarities to the β-phase are shown as colored lines on top of the structures. The dilute relaxations show structures Pu-3 through Pu-6 having considerable similarities to patterns seen in the β-phase, with Pu-3 and Pu-4 having the most distinctive similarities. These two structures' similarities to β are in agreement with their interstitials' larger formation energies, 2.617 and 2.070 eV/int dE_f, respectively, as the full transition to β would require a large formation energy.

3.2. α-Pu Interstitials – Full Relaxations

3.2.1. Energetics.

Full relaxation formation energies are shown in Table 3, with Pu-6 again being the most energetically favorable structure at 1.785 eV/int and Pu-3 being the least favorable at 2.566 eV/int. The range in E_f for the fully relaxed structures was 0.780 eV/int, suggesting that when the lattice is able to accommodate the defect, these structures are all likely to be observed experimentally due to the similar formation energies. Once fully relaxed, all defected structures yield a lower total energy than their dilute counterparts, shown as E_R in Table 3, representing the amount of strain released to get back to zero internal pressure within the lattice. This is expected as the fully relaxed structures are able to expand or contract their lattices in order to better accommodate the interstitials, thus releasing the internal pressure caused by the defect.

3.2.2. Structural Analysis.

The β unit cell is larger in most lattice parameters than our theoretical α supercell, and as such we expect to see increases in these lattice constants for the defected structures. All defected structures once fully relaxed yielded an increase in total volume, ranging from 8.11% to 11.12% expansion. The β-phase is 33.21% larger in volume than the theoretical α supercell, so these volume expansions are all expected, with the largest expansion of 11.12% being seen in Pu-2. The *a* lattice parameter changes were more variable, ranging from 1.07% contraction (Pu-3) to 6.06% expansion (Pu-4), while the *b* lattice parameter expanded for all defected structures. The most interesting changes came from the *c* lattice parameter, where all defected structures except for Pu-1 expanded by at least 1.89%. This change was not expected as the β-phase *c* lattice parameter is 27.62% less than our theoretical α cell. These results are all reported in Table 4. When comparing patterns in atom arrangement to that of the dilute relaxation structures (Figure 8), the fully relaxed structures retained a few of the same β XRD peaks as their dilute counterparts. However, Pu-4 and Pu-5 show significantly less visible β XRD peaks than their dilute structures. Shown in Figure 10, XRD results show a similar trend in Pu-4, where very few β-like peaks emerge. Pu-1 and Pu-6 follow this, each having only one distinct β-like peak, seen at $2\theta = 35.7$ and $2\theta = 35.0$, respectively. Pu-2 and Pu-5 show the greatest resemblance to β XRD peaks, with Pu-2 and Pu-5 having at least 4 and 3 distinct β peaks, respectively. This suggests that structure Pu-2 is much closer to resembling the β unit cell than the other defected structures, despite its relatively low formation energy.

3.2.3. Electronic Structure Analysis.

The partial density of states (PDOS) data was analyzed for a select number of defected structures (Pu-2 – Pu-6) that are relevant to the proposed diffusion pathways (section 3.2.4) and are shown in Figure 11. Three atoms were compared for each structure in PDOS: the interstitial atom itself (interstitial), the first nearest neighbor (1nn) to the interstitial, and that same atom in the non-defected theoretical α structure (1nn w/o defect), so we can analyze how the defect influences the electronic structure of its closest neighboring atom. Across all analyzed structures, introducing Pu interstitials as defects causes a spectral shift and broadened coupling of 6d states. 5f hybridization is weakened due to the energy required to form the interstitials, and any 5f hybridization for Pu-defected structures happens much closer to the Fermi energy than in the case for 6d states. Pu-2 exhibits very strong 6d–6d hybridization between the interstitial and its 1nn from -3.30 eV to -2.75 eV and continues past this, albeit weaker. Conversely, 5f–5f hybridization between these atoms occurs above -0.95 eV and is weak. The least energetically favorable structure (Pu-3) exhibits a very small amount of 5f–5f bonding between the interstitial and its 1nn atom from -0.90 eV to -0.54 eV, reflecting its larger E_f. More

energetically favorable structures such as Pu-5 and Pu-6 have an increased amount of 6d–6d bonding closer to the Fermi energy, suggesting that larger formation energies will shift the 6d states more towards the Fermi energy. From analysis of the PDOS, it can be stated that the d-states of interstitial atoms and their neighboring atoms will be dominant and as such, we expect to see a dominance of d-states in the β-phase as well.

3.2.4. Diffusion Pathway Proposal.

By analyzing the final relaxed positions of interstitials and by using the relative formation energies (dE_f) from the fully relaxed structures, two possible diffusion pathways are proposed, mapping out possible pathways from the theoretical α structure to the experimental β structure, as shown in Figure 9. Due to its resemblance to the β-phase in XRD and its significant amount of d-state hybridization, Pu-2 seems to show the closest resemblance to β among the other Pu-defected structures. Therefore, Pu-2 will serve as the final step in both proposed diffusion pathways. Likewise, Pu-6 continuously exhibited the lowest formation energy of interstitials and was more structurally similar to the theoretical α lattice. Pu-6 will therefore serve as the first step in both proposed pathways. These pathways will serve as a hypothesized mechanism for the α→β phase transformation for future studies.

3.3. Ga Impurities in α-Pu – Dilute Relaxations

3.3.1. Energetics.

Table 5 shows the energy results from the dilute relaxations of the Ga-defected structures. The Ga interstitial defect structures yielded a formation energy range of 3.76 eV, with INT-6a being the most favorable at 3.17 eV and INT-4b being the least favorable at 6.92 eV. These formation energies are a result of dilute relaxations and are all relatively large because of defect-induced strain. Incorporating a Ga atom into the theoretical α supercell appears to, on average, require a larger amount of energy than incorporating a Pu interstitial atom. This can be explained by analyzing the PDOS for these atoms in section 3.4.3. Ga substitutions required less energy to incorporate into the α supercell, with the least energetically favorable structure requiring only 2.47 eV (SUB-4). The most energetically favorable defect structure was SUB-6 at 1.25 eV. This suggests a formation energy range of only 1.22 eV. The small range in E_f is expected for substitutionals, as incorporation into an existing lattice site induces the least amount of strain on the lattice.

3.4. Ga Impurities in α-Pu – Full Relaxations

3.4.1. Energetics.

Only the most energetically favorable structures from the dilute relaxations were simulated for full relaxation, shown in Table 6. This includes Ga interstitial structures INT-1a, INT-6a, and INT-6b, and Ga substitutional structures SUB-6 and SUB-8. All fully relaxed structures, with the exception of SUB-8, yielded a lower formation energy than their dilute counterparts. The only unexpected result was SUB-8, which yielded a slightly higher E_f than the dilute case. The most energetically favorable among these defected structures was SUB-6 at 0.83 eV, and the least energetically favorable was interstitial structure INT-6a at 2.50 eV. It is interesting to note that INT-6a was the most energetically favorable interstitial structure in the dilute relaxations but is the least energetically favorable once allowed to fully relax. Relative energies (dE_f), shown in Table 6, were calculated relative to the SUB-6 structure. The formation energy range for all fully relaxed Ga-defected structures is 1.67 eV. As stated before, almost all Ga-defected structures after full relaxation yielded a lower E_f than the dilute case, with the exception of SUB-8. These relaxed energies are also shown in Table 6. The increase in formation energy for

SUB-8 is 0.002 eV, a 0.15% increase. This amount of formation energy increase is negligible; therefore, it can be assumed that the formation energy is the same between the dilute and fully relaxed SUB-8 structures. This implies that the internal strain caused by this substitutional was negligible, and as such an expansion of the lattice released no internal pressure [3]. All other Ga-defected structures showed a release of internal pressure once able to fully relax, with structure INT-6b releasing the most strain at -1.41 eV.

3.4.2. Structural Analysis.

Upon full relaxation, almost all Ga-defected structures show an increase in overall atomic volume from the starting theoretical α supercell (Table 7). The exception, again being SUB-8, showed a slight decrease in atomic volume by less than 0.50%, which is negligible. As stated before, this substitutional site imparts almost no strain on the lattice, and therefore requires no change in volume to incorporate the Ga atom. The remaining structures' volume changes are expected. Work from Hecker et al. shows the α' lattice to have a total volume increase of 1.82% from α [1]. The closest defected structure to this result is SUB-6 at 1.18%. All fully relaxed Ga-defected structures show XRD patterns very similar to that of the theoretical α supercell, as shown in Figure 12. These XRD patterns were also compared to an experimental α' supercell, constructed in the same manner as the theoretical α supercell, using a 1 x 2 x 1 α' unit cell [1]. There are not enough noticeable similarities between the Pu–Ga structures and the theoretical α' XRD patterns to draw conclusions from, but the expansion of lattice constants seen in these structures is promising.

3.4.3. Electronic Structure Analysis.

PDOS data from structure INT-6a unfortunately shows no noticeable electronic structure changes upon introduction of the Ga defect into the lattice, suggesting that a Ga interstitial at this site does not cause significant interactions between valence electrons with neighboring Pu atoms. Conversely, both INT-1a and INT-6b show very strong hybridizations between the 4p states of the Ga interstitials and the 7s, 6d, and 5f states of their 1nn Pu atoms. For INT-1a, hybridization can be seen with the 7s, 6d and 5f states in a two-peak structure from -2.12 eV to -1.79 eV, with 4p–7s hybridization starting at -1.67 eV and ending at -2.12 eV. The 4p–7s hybridization can also be seen from -3.24 eV to -2.43 eV, keeping hybridizations of these valence shells further away from the Fermi energy. There is only a small amount of hybridization near the Fermi energy, seen in the 5f valence shell, hybridizing with the 4p shell of the Ga interstitial from -0.24 eV up to the Fermi energy. This result is in agreement with PDOS analysis from interstitial Pu structures (Pu2 – Pu6), where 5f hybridization occurred rarely and only very close to the Fermi energy. The most significant observation of INT-1a PDOS results is the 4p–6d hybridization, which can be observed from -4.00 eV all the way to -1.79 eV, with none of this hybridization occurring before the interstitial is introduced, suggesting that 4p–6d hybridization is heavily preferred for an interstitial in this site. Looking at structure INT-6b, in the range of -3.14 eV to -2.35 eV, the 7s and 6d states show several peaks that line up with those from the 4p states of the Ga interstitial, again suggesting a preference toward hybridizations further from the Fermi energy for these valence shells. The 4p–5f hybridization is present from -2.78 eV to -2.43 eV but is much broader. This also agrees with results from the Pu interstitial structures (Pu-2 – Pu-6) where 5f bonding was much less favorable. As for structures SUB-6 and SUB-8, SUB-6 shows a strong two-peak hybridization of 4p–6d states from -3.24 eV to -2.68 eV, again far from the Fermi energy. The 7s and 5f states have little to no hybridizations with the 4p states from the Ga substitutional atom. In structure SUB-8, however, 4p–5f hybridization appears alongside the two-peak hybridization of 4p–6d found in SUB-6. The addition of 5f bonding here aligns with SUB-8's higher formation energy (0.585 eV higher), as it has been concluded

that 5f hybridization is less favorable for the introduction of defects in α-Pu. Electronic structure data for all fully relaxed Ga-defected structures can be found in Figure 13.

4. Conclusions

By exploring the energetics, structural changes, and electronic changes induced by Pu or Ga interstitials and substitutionals in the α-Pu lattice, we have identified the potential mechanisms of the transition from α-Pu to β-Pu, and how Ga may influence the martensitic phase transition to the α' lattice. Pu atoms at interstitial sites 2 – 6 cause ionic relaxations and overall lattice volume changes reflecting patterns seen in the β phase, while also significantly shifting hybridization of 6d states further from the Fermi energy. Relative formation energy data suggest possible diffusion pathways to β via defect structures Pu-2 through Pu-6. Ga atoms at interstitial sites 1a, 6a, and 6b within the α lattice produce significant lattice expansions, while a Ga atom substituted in Pu site 6 produces a more subtle expansion that is also seen in the α' lattice [1]. PDOS data reveals that Ga interstitials in sites 6a and 6b influence bonding between the 4p states of the Ga atom and the 7s, 6d, and 5f states of its closest Pu atom. Additionally, a Ga atom substituted in site 8 will influence 4p–5f hybridization, resulting in a much larger formation energy for the defect. Additional research will be needed to further analyze bonding patterns and structural changes caused by the introduction of defects, including simulation of additional defected structures as well as data derived from experiment.

5. Acknowledgements

This work was supported by the LDRD-Seaborg Institute Director's Initiative project #20210795DI and LDRD-DR project #20210001DR. This research used resources provided by the Los Alamos National Laboratory Institutional Computing Program, which is supported by the U.S. Department of Energy National Nuclear Security Administration under Contract No. 89233218CNA000001. Support and guidance of this work from my mentor Sarah C. Hernandez (MST-16), and discussions with Avadh Saxena (T-4), Franz Freibert (Seaborg Institute), Charles Fricke (MST-16), and Raymond Atta-Fynn (MST-16).

6. Figures and Tables

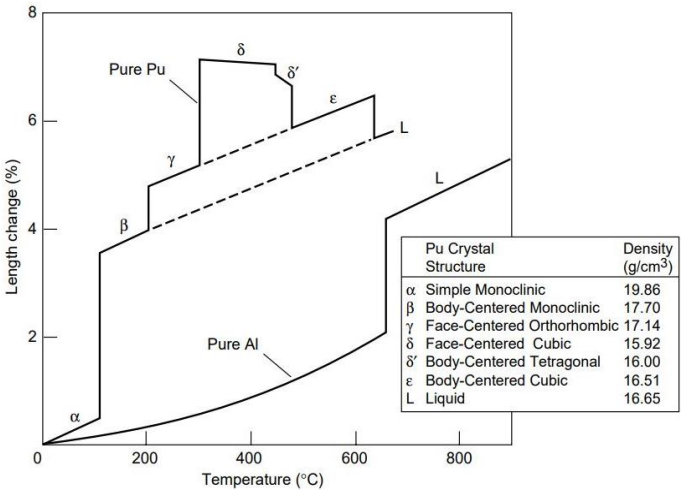

Figure 1. Phase diagram of solid plutonium, showing each of the six solid-state phases, melting points, length changes, and densities compared to pure aluminum. Image from Hecker et al [1].

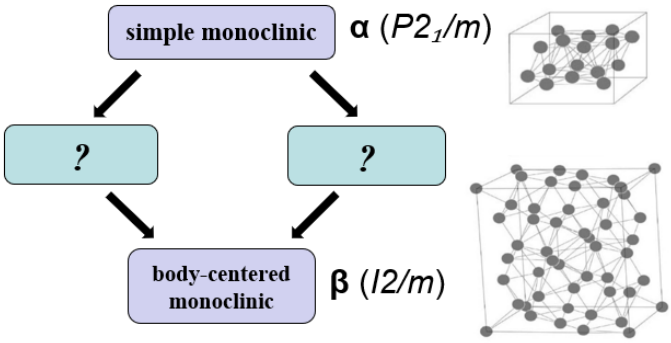

Figure 2. Visual representation of the unknown mechanism for transition between α-Pu and β-Pu. The aim of this research is to uncover more information regarding the possible transition states between the two (shown as blue boxes). Unit cell images from Zocco et al [8].

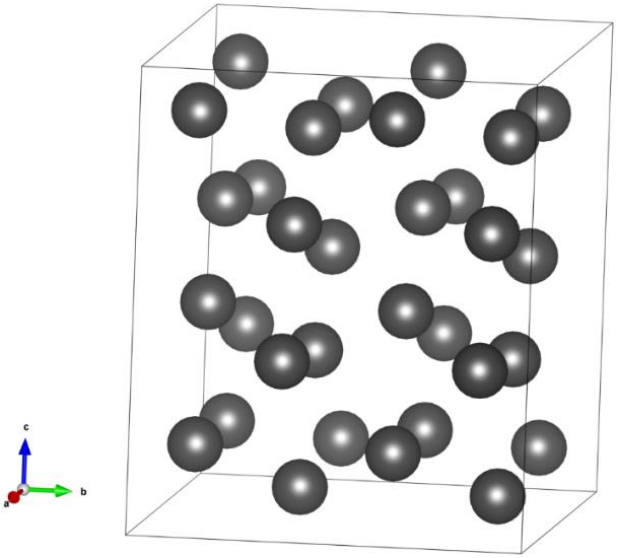

Figure 3. 1 x 2 x 1 α-Pu supercell, constructed to better replicate the structure parameters of the β unit cell.

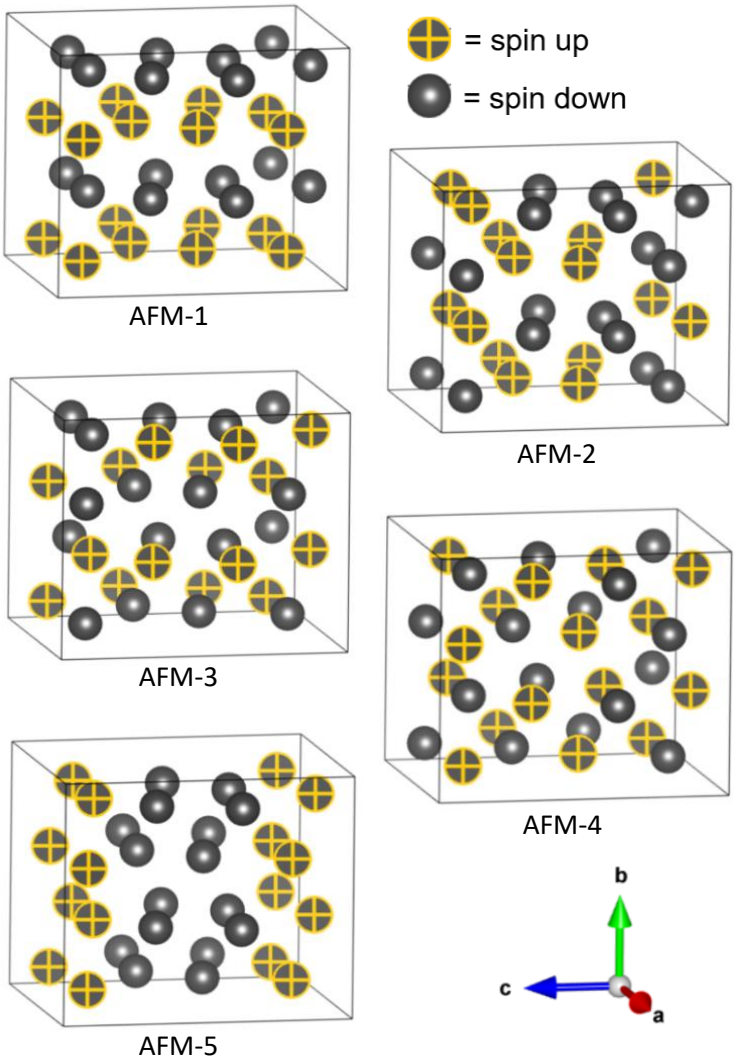

Figure 4. Each of the five proposed AFM arrangements for the α-Pu supercell. Yellow markings indicate atoms aligned magnetically opposite to the others.

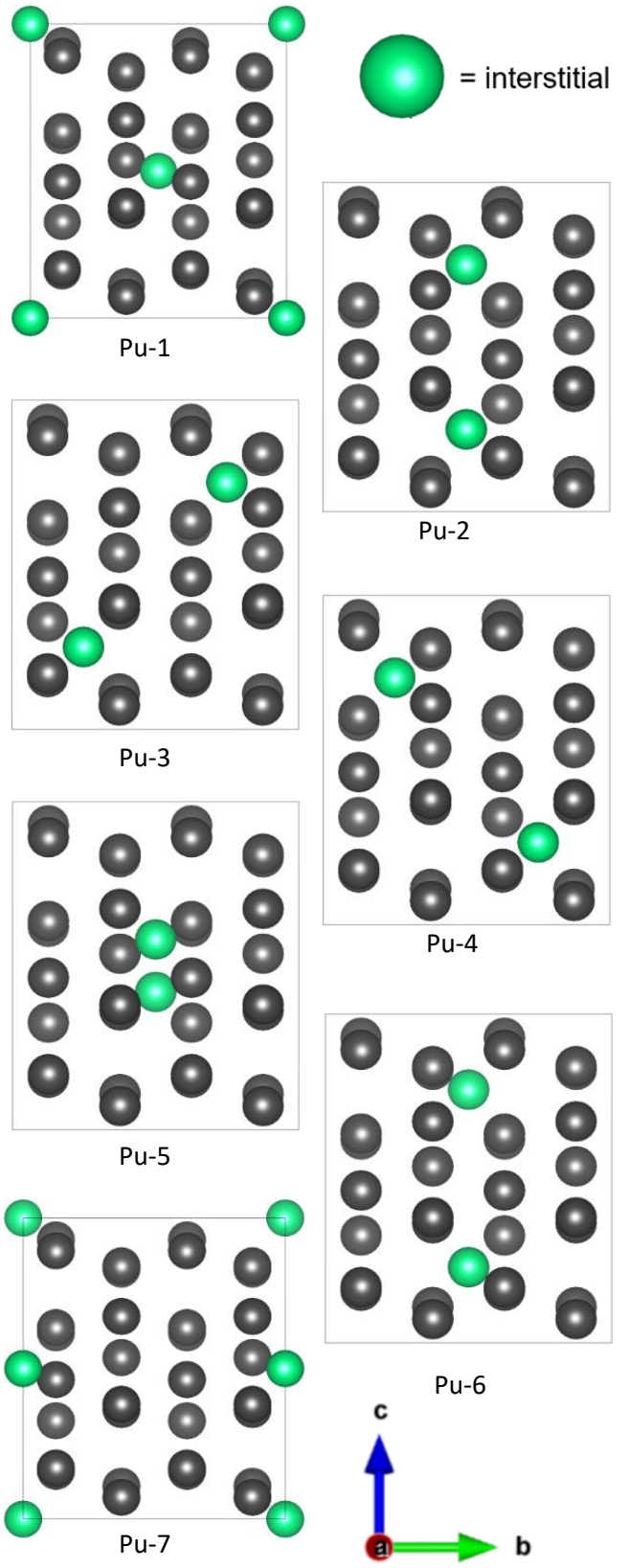

Figure 5. Each of the seven proposed interstitial structures for Pu interstitials in the theoretical α supercell. Two interstitials (green) are placed in each structure. Note: Pu-2 and Pu-6 differ in a-axis coordinates.

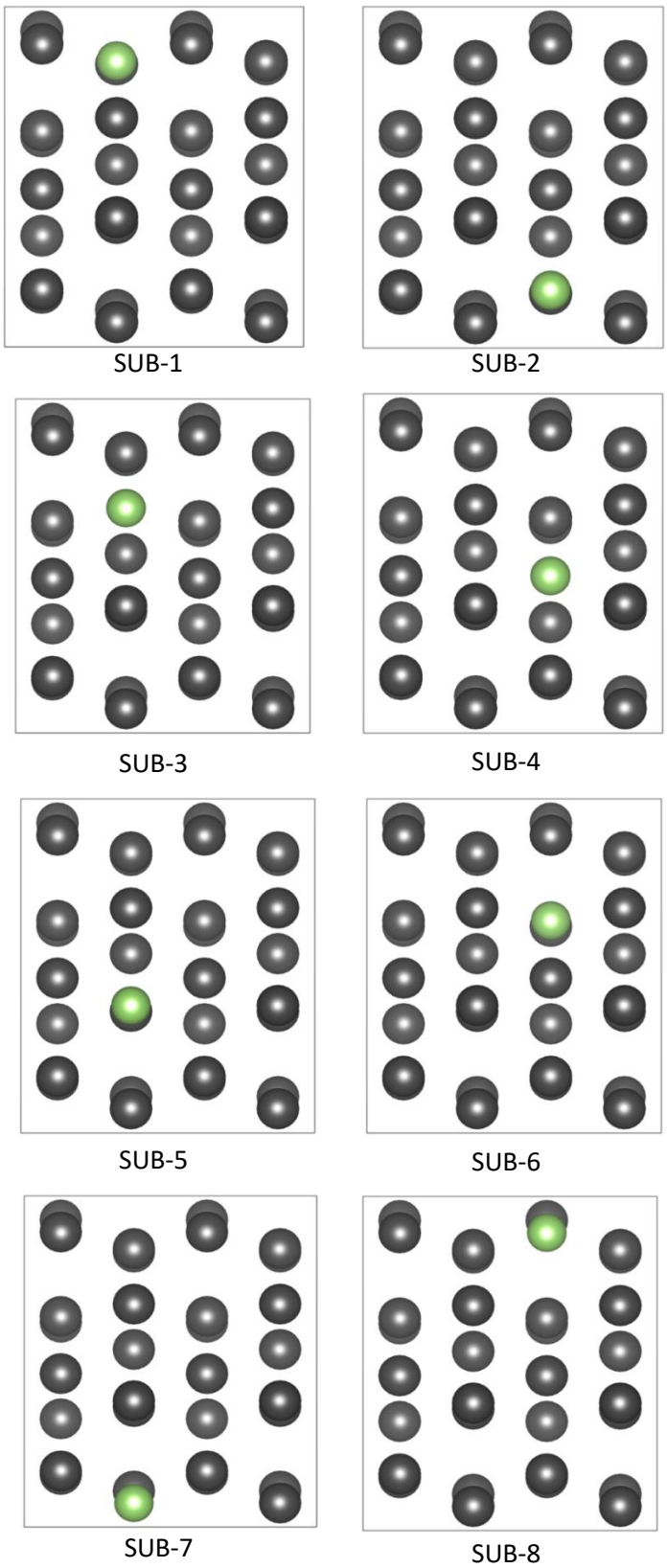

Figure 6. Each of the eight proposed Pu–Ga alloys made by substituting a Ga atom (green) in each of the eight symmetric lattice sites of the theoretical α supercell.

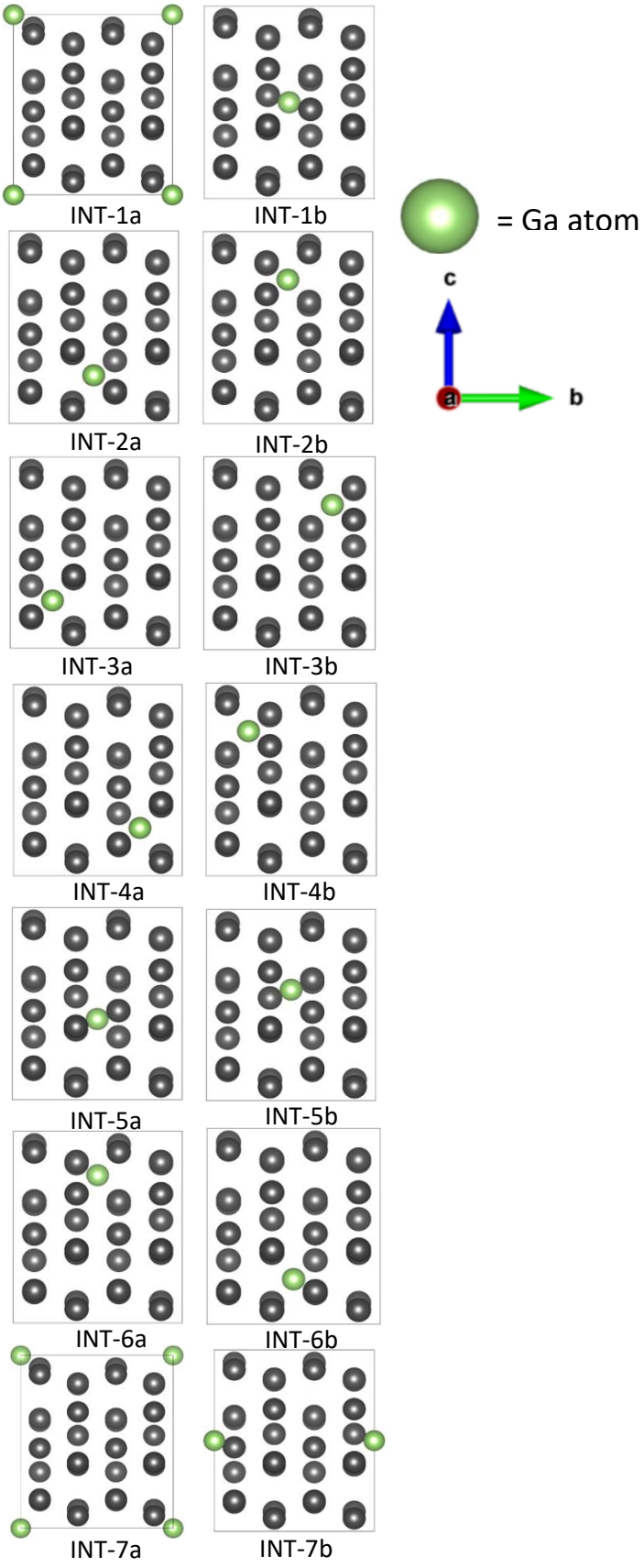

Figure 7. Using the same interstitial sites as suggested for Pu interstitials, 14 Pu–Ga structures were proposed with one Ga atom at each interstitial site.

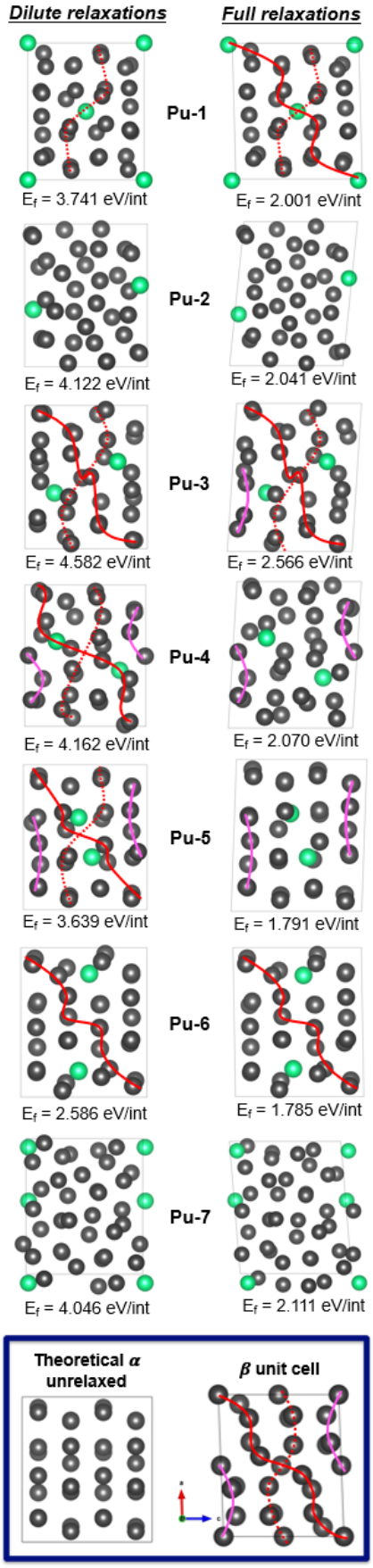

Figure 8. Pu interstitial structures after dilute and full relaxations. Colored lines indicate similarities to ion arrangements seen in the β unit cell.

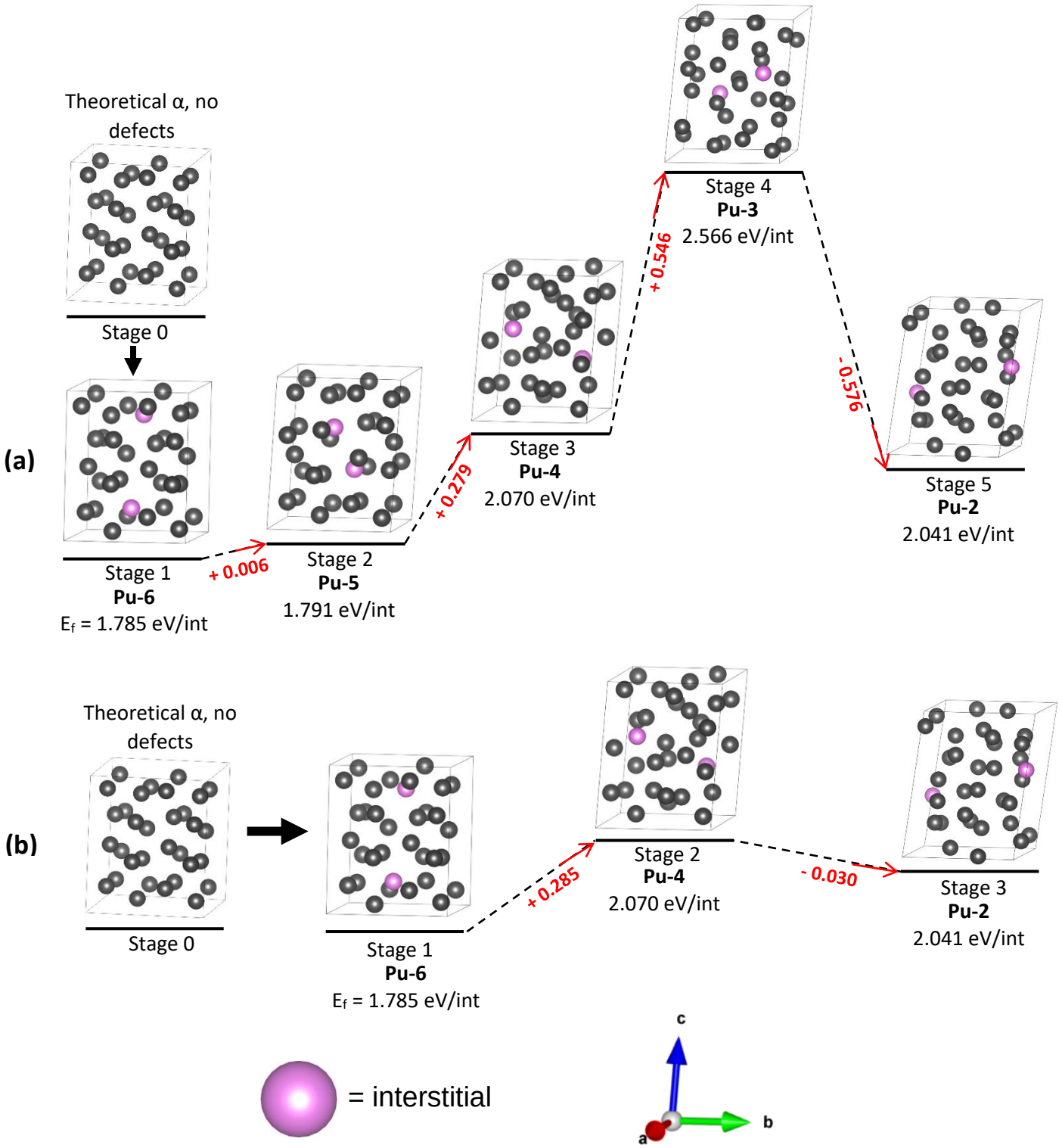

Figure 9. Formation and potential diffusion of two Pu interstitials through the theoretical α supercell via two different possible pathways (**a** – **b**).

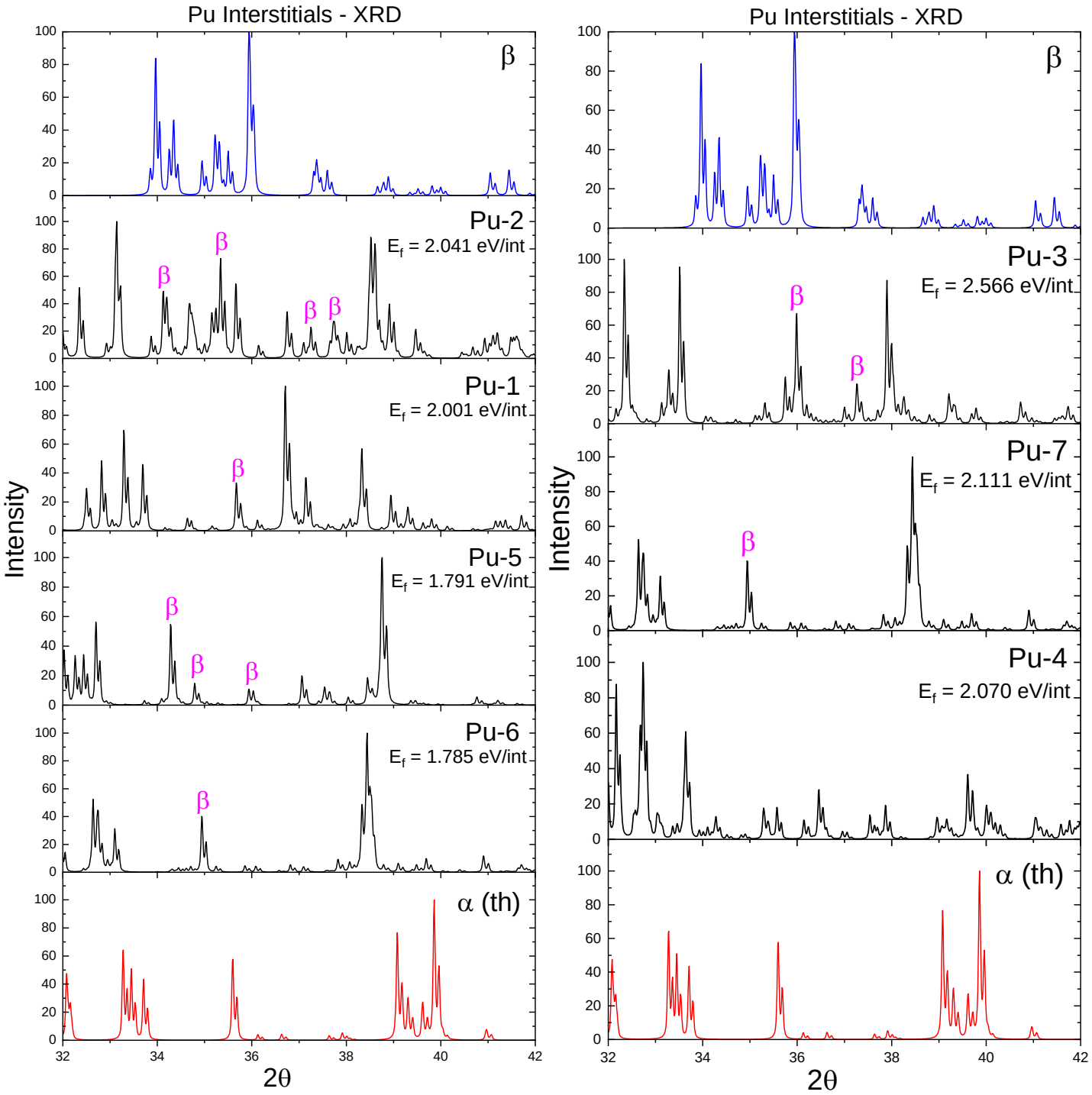

Figure 10. XRD patterns from fully relaxed Pu interstitial structures, compared to XRD for the experimental β unit cell and the theoretical α supercell, arranged in order of formation energy. Peaks similar to β are highlighted with pink text.

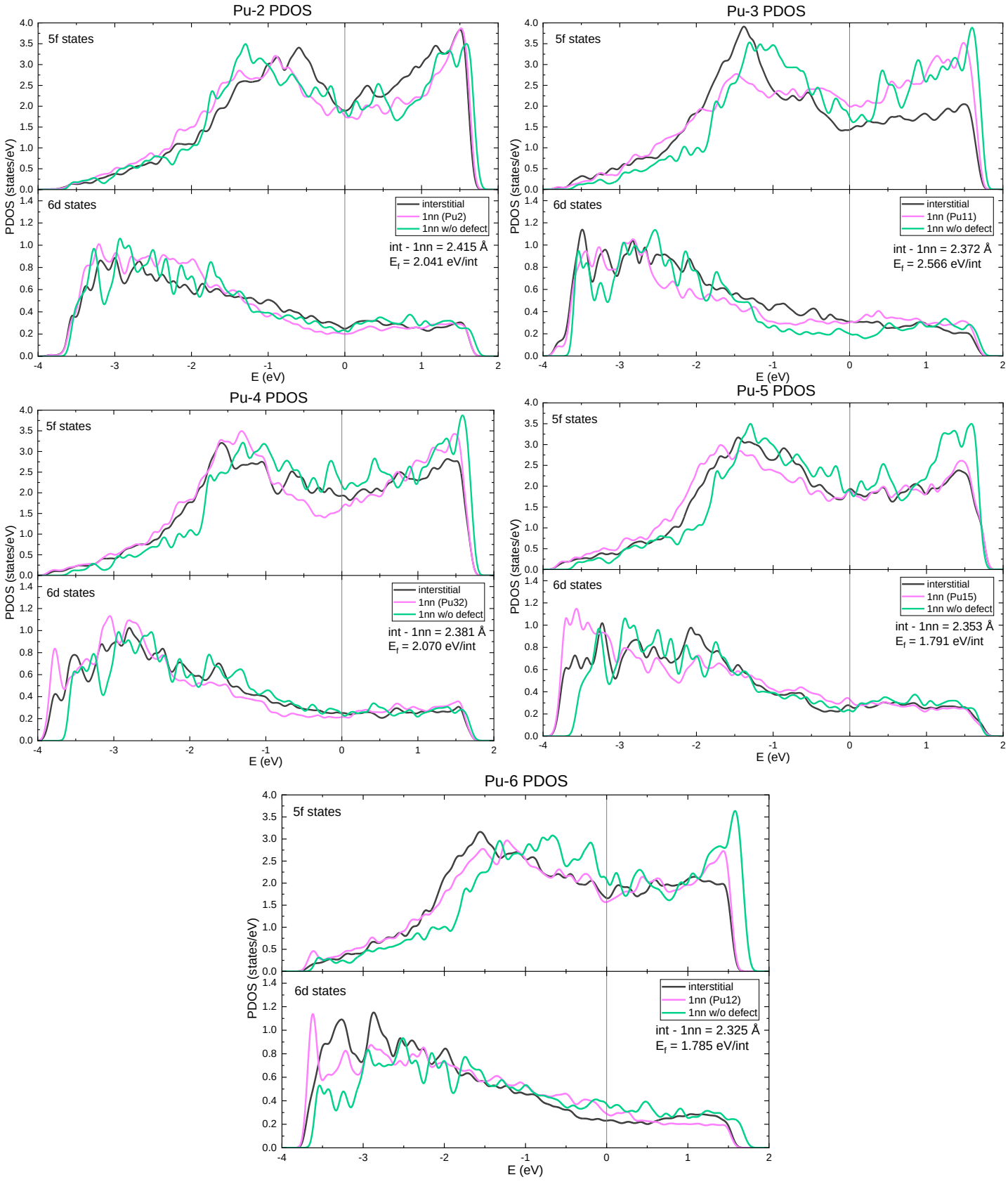

Figure 11. PDOS data for five of the fully relaxed Pu interstitial structures. These five structures are used in the proposed diffusion pathways (Figure 9). For each structure, the interstitial atom's 6d and 5f states are compared to that of its first nearest neighbor (1nn) and that same atom in the non-defected theoretical supercell (1nn w/o defect).

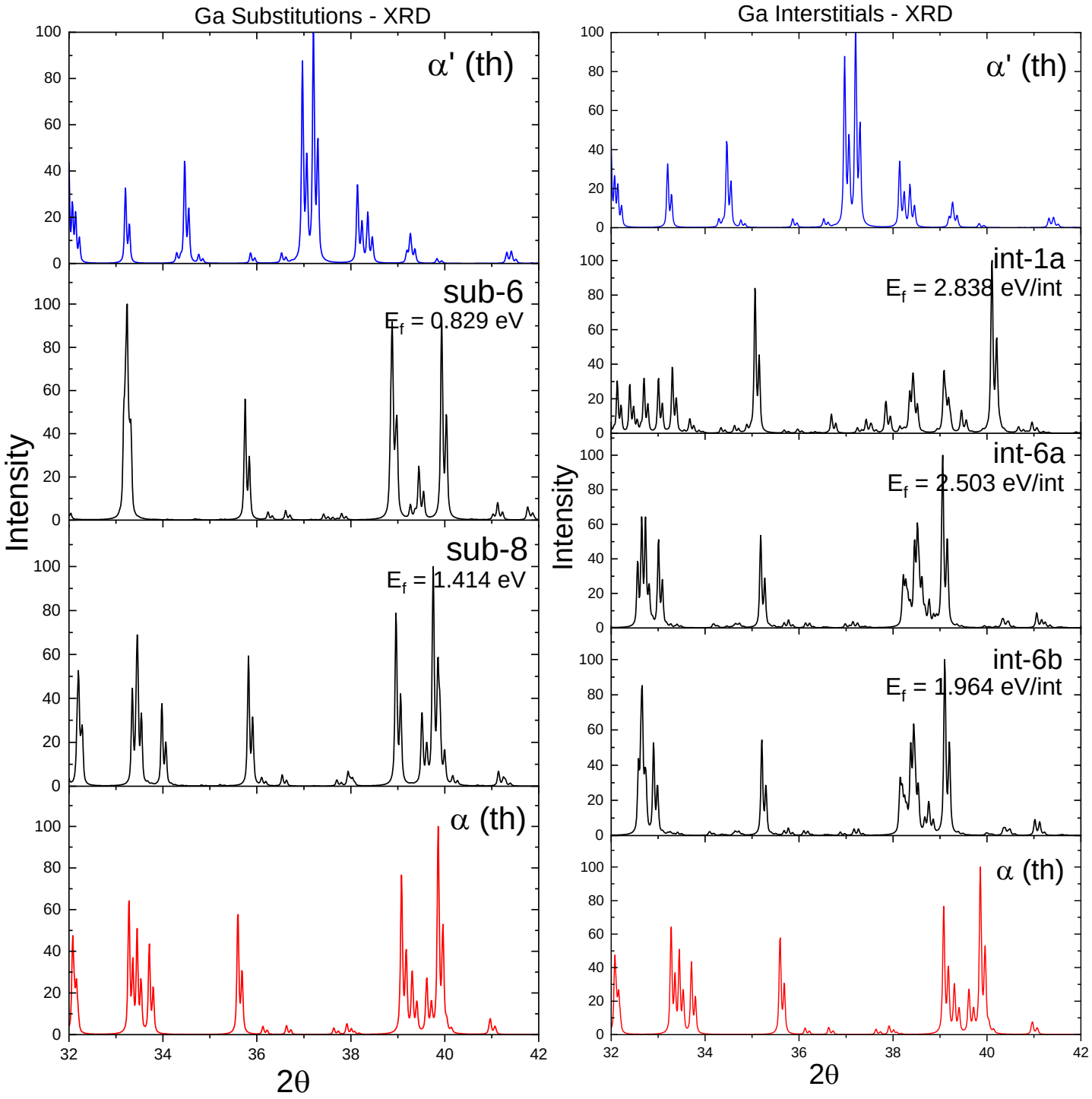

Figure 12. XRD patterns for fully relaxed Pu-Ga structures, compared to the theoretical α supercell and the 1x2x1 experimental α' supercell. Note: α' unit cell data was obtained from the research done by Hecker et al [1].

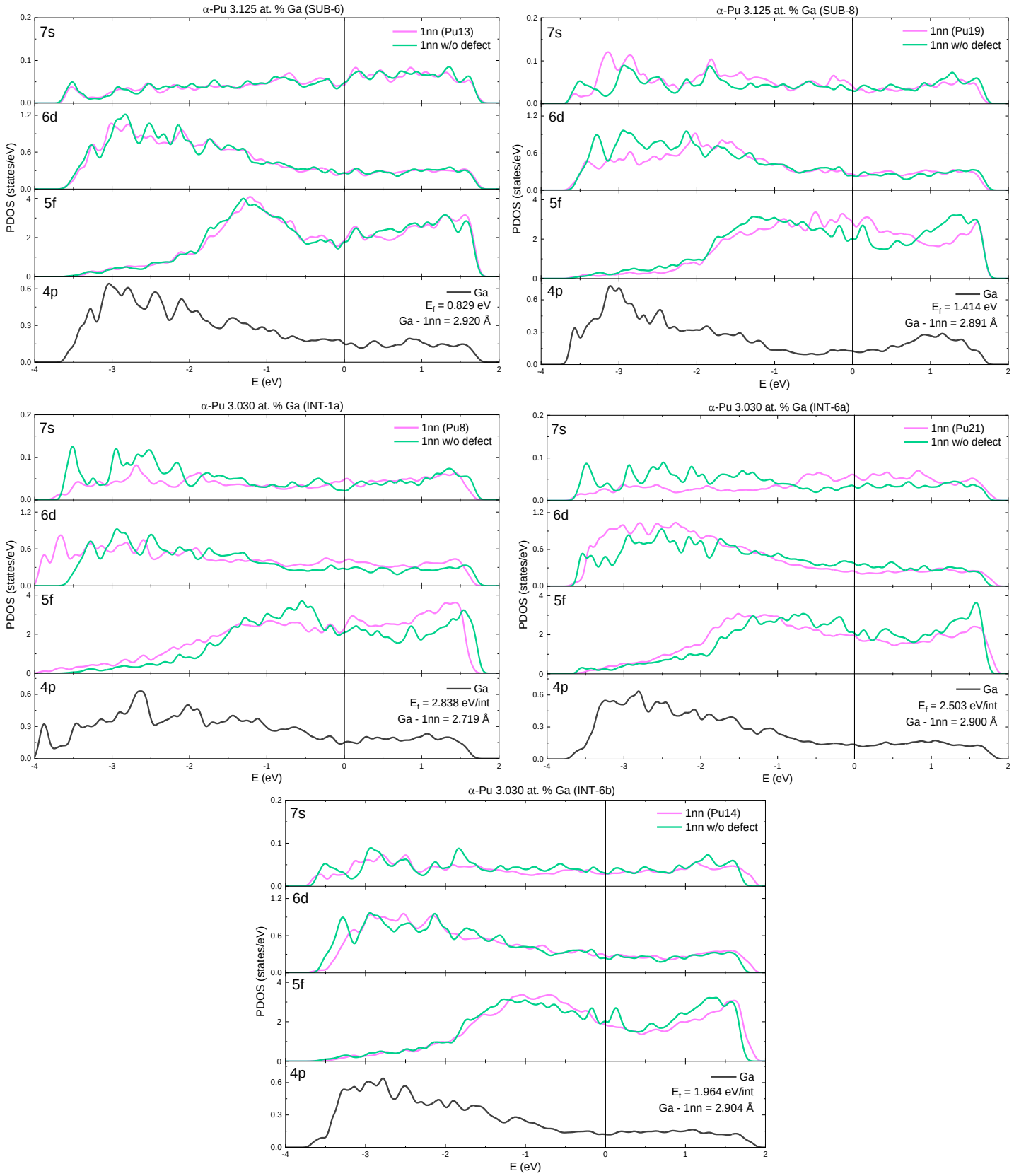

Figure 13. PDOS data for fully relaxed Pu–Ga alloys. The 4p states of each Ga defect are compared to the 5f, 6d, and 7s states of its first nearest neighbor (1nn) and that same atom in the non-defected theoretical α supercell (1nn w/o defect).

Table 1. Results from proposed AFM arrangements of the 1 x 2 x 1 α supercell, including ground-state energies and volume changes for each.

Structure	E_0 (eV)	dV (%)
AFM-1	***-461.416***	-11.362
AFM-2	***-462.278***	-11.624
AFM-3	***-461.916***	-10.781
AFM-4	***-461.359***	-11.886
AFM-5	***-462.744***	-10.502

Table 2. Energy data from dilute relaxations of Pu interstitial structures, where E_f is the formation energy per interstitial and dE_f is the relative formation energies compared to the most energetically favorable structure (Pu-6).

Structure	E_f (per int)	dE_f (eV)
Pu-1	3.741	***1.155***
Pu-2	4.122	***1.537***
Pu-3	4.582	***1.996***
Pu-4	4.162	***1.576***
Pu-5	3.639	***1.053***
Pu-6	2.586	***0.000***
Pu-7	4.046	***1.460***

Table 3. Energy data from full relaxations of Pu interstitial structures. E_R is the relaxed energy, or the difference in E_0 from the dilute relaxations.

Structure	E_f (per int)	dE_f (eV)	E_R (eV)
Pu-1	2.001	***0.216***	***-3.570***
Pu-2	2.041	***0.256***	***-4.163***
Pu-3	2.566	***0.780***	***-3.931***
Pu-4	2.070	***0.285***	***-4.184***
Pu-5	1.791	***0.006***	***-3.696***
Pu-6	1.785	***0.000***	***-1.601***
Pu-7	2.111	***0.326***	***-3.870***

Table 4. Structure changes of fully relaxed Pu interstitial structures relative to the theoretical α supercell parameters. These values for the experimental β unit cell are also shown for reference.

Structure	dV (%)	da (%)	db (%)	dc (%)	dα (%)	dβ (%)	dγ (%)
Pu-1	***9.751***	1.300	8.436	-0.288	2.220	-1.034	-3.278
Pu-2	***11.118***	0.069	1.384	10.580	-7.439	0.086	5.834
Pu-3	***10.542***	-1.072	5.166	9.280	-3.900	5.613	0.670
Pu-4	***7.961***	6.057	0.978	1.885	-2.760	1.720	-3.954
Pu-5	***9.976***	3.877	2.831	3.121	-1.777	0.163	-1.769
Pu-6	***7.525***	0.959	3.568	2.931	1.205	0.188	-0.855
Pu-7	***8.106***	-0.366	3.309	6.700	4.820	2.938	0.791
BETA (exp)	***33.207***	55.717	15.751	-27.620	0.002	-9.538	-0.002

Table 5. Energy data from dilute relaxations of Pu-Ga structures.

Structure	E_f (per int)	dE_f (eV)
SUB-1	2.274	***1.026***
SUB-2	2.086	***0.838***
SUB-3	1.605	***0.357***
SUB-4	2.465	***1.217***
SUB-5	1.989	***0.741***
SUB-6	1.248	***0.000***
SUB-7	1.490	***0.242***
SUB-8	1.412	***0.165***
INT-1a	3.572	***0.406***
INT-1b	6.708	***3.542***
INT-2a	4.512	***1.346***
INT-2b	6.064	***2.898***
INT-3a	4.609	***1.443***
INT-3b	5.546	***2.380***
INT-4a	5.509	***2.343***
INT-4b	6.921	***3.755***
INT-5a	4.444	***1.278***
INT-5b	3.899	***0.733***
INT-6a	3.166	***0.000***
INT-6b	3.374	***0.208***
INT-7a	4.845	***1.679***
INT-7b	6.147	***2.981***

Table 6. Energy data from full relaxations of Pu-Ga structures.

Structure	E_f (per int)	dE_f (eV)	E_R (eV)
SUB-6	0.829	***0.000***	***-0.419***
SUB-8	1.414	***0.585***	***0.002***
INT-1a	2.838	***2.009***	***-1.061***
INT-6a	2.503	***1.674***	***-0.663***
INT-6b	1.964	***1.135***	***-1.410***

Table 7. Structure changes of fully relaxed Pu–Ga alloys relative to the theoretical α supercell.

Structure	dV (%)	da (%)	db (%)	dc (%)	dα (%)	dβ (%)	dγ (%)
SUB-6	***1.181***	-0.226	-0.179	1.215	-0.001	-1.043	-0.014
SUB-8	***-0.433***	0.080	0.257	-0.923	0.007	-0.432	-0.007
INT-1a	***3.381***	0.896	-0.524	2.969	2.213	-0.263	0.205
INT-6a	***5.867***	0.824	1.844	2.839	0.119	-0.703	-0.173
INT-6b	***5.973***	0.814	1.860	2.921	0.114	-0.748	-0.167

5. References

[1] S. S. Hecker, "Plutonium and its alloys," *Los Alamos Science*, no. 26, p. 290, 2000.

[2] M. A. Boring and J. L. Smith, "Plutonium Condensed-Matter Physics: A survey of theory and experiment," *Los Alamos Science*, no. 26, p. 90, 2000.

[3] B. Sadigh and W. G. Wolfer, "Gallium stabilization of delta-Pu: Density-functional calculations," *Physical Review B*, no. 72, 2005.

[4] K. T. Moore, C. R. Krenn, M. A. Wall and A. J. Schwartz, "Orientation Relationship, Habit Plane, Twin Relationship, Interfacial Structure, and Plastic Deformation Resulting from the delta to alpha prime Isothermal Martensitic Transformation in Pu-Ga Alloys," *Metallurgical and Materials Transactions A*, no. 38A, p. 686, 2007.

[5] K. J. M. Blobaum, J. R. Jeffries, A. J. Schwartz, H. Cynn, W. Yang, M. A. Wall and W. J. Evans, "In situ X-ray diffraction study of the δ to α′ isothermal martensitic transformation kinetics in a Pu–Ga alloy," *Journal of Nuclear Materials*, vol. 412, no. 3, p. 327, 2011.

[6] P. Deloffre, J. L. Truffier and A. Falanga, "Phase transformation in Pu–Ga alloys at low temperature and under pressure: limit stability of the δ phase," *Journal of Alloys and Compounds*, Vols. 271-273, p. 370, 1998.

[7] T. E. Mitchell, J. P. Hirth, D. S. Schwartz and J. N. Mitchell, "The beta to alpha phase transformation in plutonium," *Acta Materialia*, no. 61, p. 2895, 2013.

[8] T. G. Zocco, D. S. Schwartz and J. Park, "Investigation of plutonium allotropic phase transformations through differential scanning calorimetry," *Journal of Nuclear Materials*, vol. 353, no. 1-2, p. 119, 2006.

[9] S. C. Hernandez and F. J. Freibert, "Ab Initio Study of the Effect of Mono-Vacancies on the Metastability of Ga-Stabilized delta-Pu," *Applied Sciences*, no. 10, 2020.

[10] A. Landa, P. Soderlind and L. Vitos, "Density-functional calculations of α-Pu–Ga(Al) alloys," *Journal of Alloys and Compounds*, Vols. 444-445, p. 296, 2007.

[11] J. G. Lee, Computational Materials Science : An Introduction, Second Edition, Boca Raton, FL: Taylor & Francis Group, LLC, 2017.

[12] D. S. Scholl and J. A. Steckel, Density Functional Theory : A Practical Introduction, Hoboken, NJ: John Wiley & Sons, Inc., 2009.

[13] P. Hohenberg, W. Kohn, “Inhomogeneous Electron Gas,” *Physical Review*, vol. 136, no. 3B, p. 864, 1964.

[14] J. P. Perdew, K. Burke and M. Ernzerhof, "Generalized Gradient Approximation Made Simple," *Physical Review Letters*, vol. 77, p. 3865, 1996.

[15] G. Kresse and J. Hafner, "Ab initio molecular dynamics for liquid metals," *Physical Review B*, vol. 47, p. 558, 1993.

[16] G. Kresse and J. Hafner, "Ab initio molecular-dynamics simulation of the liquid-metal–amorphous semiconductor," *Physical Review B*, vol. 49, 1994.

[17] G. Kresse and J. Furthmuller, "Efficiency of ab-initio total energy calculations for metals and semiconductors," *Computational Materials Science*, vol. 54, 1996.

[18] G. Kresse and J. Furthmuller, "Efficient iterative schemes for ab initio total-energy calculations using a plane-wave," *Physical Review B*, vol. 54, 1996.

[19] H. J. Monkhorst, J. D. Pack, “Special points for Brillouin-zone integrations,” *Physical Review B*, vol. 13, no. 12, p. 5188, 1976.

[20] S. C. Hernandez, A. K. Ray, C. D. Taylor, “Quantum size effects in alpha-plutonium (020) surface layers,” *Solid State Communications*, vol. 172, p. 29, 2013.

[21] J. C. Lashley, A. Lawson, R. J. McQueeney and G. H. Lander, "Absence of magnetic moments in plutonium," *Physical Review B*, vol. 72, 2005.

[22] B. Sadigh, P. Soderlind and W. G. Wolfer, "Geometry and electronic structure of alpha-Pu: A theoretical study," *Physical Review B*, vol. 68, 2003.

[23] K. Momma, F. Izumi, “*VESTA* 3 for three-dimensional visualization of crystal, volumetric and morphology data,” *Journal of Applied Crystallography*, vol. 44, p. 1272, 2011.

[24] *OriginPro 2021b*, OriginLab Corporation, 2021.